Eleven-Membered Fused-Ring Low Band-Gap Polymer with Enhanced Charge Carrier Mobility and Photovoltaic Performance

Yongxi Li, Kai Yao, Hin-Lap Yip, Fei-Zhi Ding, Yun-Xiang Xu, Xiaosong Li, Yu Chen, and Alex K.-Y. Jen**

A multi-ring, ladder-type low band-gap polymer (PIDTCPDT-DFBT) is developed to show enhanced light harvesting, charge transport, and photovoltaic performance. It possesses excellent planarity and enhanced effective conjugation length compared to the previously reported fused-ring polymers. In order to understand the effect of extended fused-ring on the electronic and optical properties of this polymer, a partially fused polymer PIDTT-T-DFBT is also synthesized for comparison. The fully rigidified polymer provides lower reorganizational energy, resulting in one order higher hole mobility than the reference polymer. The device made from PIDTCPDT-DFBT also shows a quite promising power conversion efficiency of 6.46%. Its short-circuit current (14.59 mA cm^{-2}) is also among the highest reported for ladder-type polymers. These results show that extending conjugation length in fused-ring ladder polymers is an effective way to reduce band-gap and improve charge transport for efficient photovoltaic devices.

1. Introduction

Recently, the vigorous development of donor–acceptor (D–A) alternating conjugated polymers has resulted in the rapid advancement of polymer solar cells (PSCs), with power conversion efficiency (PCE) reaching over 9% in single-junction cells.[1] While the molecular design of new semiconducting materials has played a crucial role in enhancing the efficiency of these devices, it is important to further improve their light-harvesting and charge-transporting properties in order to use them for practical applications. Especially, there is a need to develop polymers with good processibility but more rigidified structures to reduce reorganization energy for improving charge mobility. In addition, they need to have broader absorption and ambient stability.[2]

Among various donor materials developed for bulk-heterojunction (BHJ) devices, the multi fused-ring ladder-type conjugated polymers are quite attractive due to their superior optical and electrical properties.[3–8] The results from Cheng, McCulloch, and Jen[9–17] have shown that extending the conjugation length of the ladder-type donor unit will facilitate π-electron delocalization along the polymer backbone, which provides an effective way to reduce their band-gap. In addition, the more rigid, coplanar structures of these polymers can also prevent rotational disorder to reduce reorganization energy, which may contribute to enhanced charge separation and carrier mobility.

The cyclopenta[2,1-b;3,4-b']dithiophene (CPDT) based conjugated polymers are quite interesting due to their red-shifted absorption and excellent hole-transporting properties.[18,19] However, due to very strong electron-donating ability of the CPDT unit, these polymers often have quite high-lying molecular orbital energy levels, which limit the ability to achieve optimal open-circuit voltage (V_{oc}) in the resultant devices.[20] In addition, the CPDT-based polymers exhibit strong packing nature, which significantly impacts their processibility.[21] To alleviate these problems, Cheng has recently developed a new donor unit BDCPDT with two CPDT units separated by a central benzene unit.[17] The polymer made with this donor showed lower HOMO level and better solubility compared to those of CPDT-based polymers, which contributed to higher device performance. However, the main drawback of this polymer is its wide optical band gap (1.88 eV), which reduces its light-harvesting ability and photocurrent generation.

It would be ideal if CPDT can be fused with proper ladder-type units to make low band-gap polymers with high charge carrier mobility and good processibility. In this article, we have synthesized a multi-ring indacenodithiophene-biscyclopentadithiophene (IDTCPDT) donor, where the central IDT core is fused with two CPDT units (**Scheme 1**). This large-sized

Y. X. Li, K. Yao, Dr. H.-L.Yip,
Dr. Y.-X. Xu, Prof. Dr. A. K.-Y. Jen
Department of Materials Science and Engineering
University of Washington
Seattle, WA 98195, USA
E-mail: ajen@u.washington.edu
Y. X. Li, Prof. Dr. Y. Chen
Key Lab for Adv. Mater.
Institute of Applied Chemistry
East China University of Science and Technology
130 Mei Long Road, Shanghai 200237, China
E-mail: chentangyu@yahoo.com
F.-Z. Ding, Prof. X. Li
Department of Chemistry
University of Washington
Box 351700, Seattle, WA 98195, USA

DOI: 10.1002/adfm.201303953

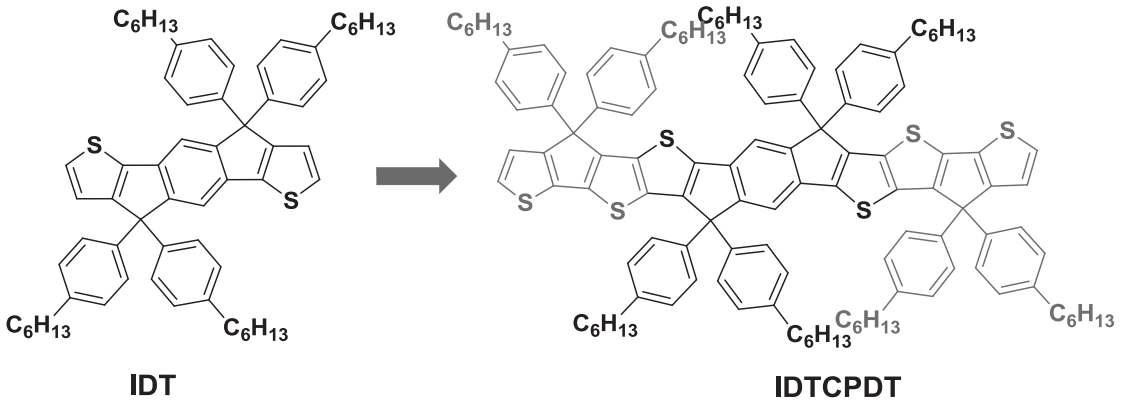

Scheme 1. The chemical structures of IDT and IDTCPDT.

donor can result in polymers with extended conjugation length and decreased HOMO energy level. This will reduce band-gap without significantly sacrificing V_{OC} in devices. To ensure good processibility, we have introduced eight side-chains on the highly coplanar aromatic/heteroaromatic rings. In order to understand the effect of rigidified structure on electronic and optical properties of the polymer, we have also synthesized a reference polymer, PIDTT-T-DFBT, which has two thiophene spacers without being fused between indacenodithieno[3,2-b]thiophene (IDTT) and difluorobenzothiadiazole (DFBT) for direct comparison. The chemical structures and the synthetic routes used to make PIDTT-T-DFBT and PIDTCPDT-DFBT are depicted in **Scheme 2**

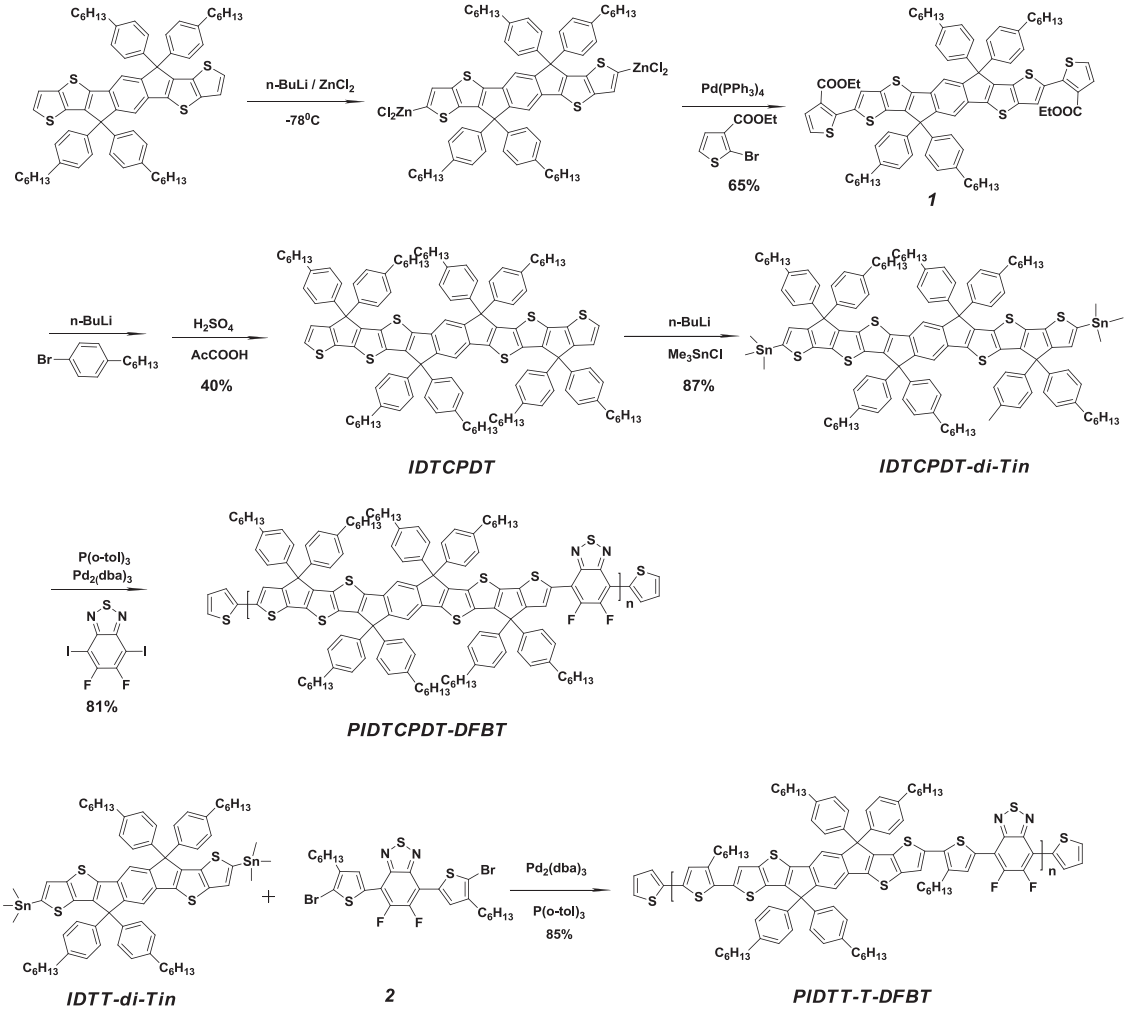

Scheme 2. The chemical structures and synthesis routes of PIDTCPDT-DFBT and PIDTT-T-DFBT.

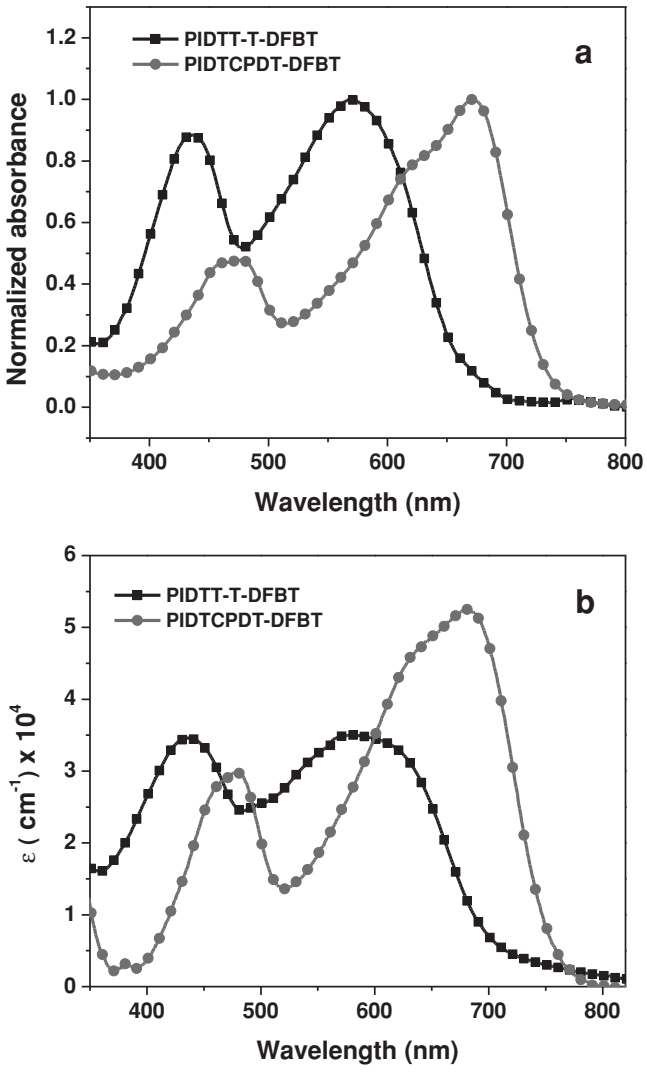

Figure 1. a) The normalized UV-Vis spectra of PIDTT-T-DFBT and PIDTCPDT-DFBT in chlorobenzene solution and b) the extinction coefficients of polymer films.

2. Results and Discussion

The palladium-catalyzed coupling between 2-bromo-thiophene-3-ehthylcarboxylate with IDTT zinc chloride (generated in-situ through trans-metalation of lithiated IDTT with zinc chloride) afforded compound **1** in a 65% yield. (Scheme 2) After a nucleophilic addition reaction with p-hexylphenyllithium and an acid-promoted intramolecular annulation, IDTCPDT could be isolated in 40% yield. The mixture was further lithiated and quenched with trimethyltin chloride to afford IDTCPDT-di-Tin in 87% yield. Finally, PIDTCPDT-DFBT and PIDTT-T-DFBT were obtained by copolymerizing IDTCPDT-di-Tin and IDTT-di-tin with di-iodo-DFBT and di-bromo-DTDFBT, respectively. The resulting polymers can be dissolved in chlorinated solvents, such as chlorobenzene (CB) and dichlorobenzene (DCB), but PIDTT-T-DFBT has much lower solubility in chloroform ($CHCl_3$). The number-average molecular weight (M_n) of PIDTCPDT-DFBT was 19.6 kDa with a polydispersity index (PDI) of 2.15, while PIDTT-T-DFBT had an M_n of 17.3 kDa, with a PDI of 1.90. No distinct thermal transitions could be detected between RT and 280 °C by DSC measurements, which indicates these polymers have similar amorphous characteristics like other IDT-based polymers.[22,23]

The optical absorption of the polymers was investigated both in CB solutions and in thin films, with the results shown in **Figure 1** and summarized in **Table 1**. Both polymers exhibit two strong absorption bands, with a shorter wavelength band due to π–π^* transitions, and a longer wavelength band due to intramolecular charge transfer (ICT) (Figure 1a). PIDTCPDT-DFBT exhibits a much stronger ICT compared to that of PIDTT-T-DFBT, accompanied by a significantly red-shifted absorption. This is likely due to the stronger electron-donating ability of the IDTCPDT unit as well as increased effective conjugation length and reduced rotational disorder of the polymer chains. The band-gaps extracted from their absorption band edges are 1.73 eV and 1.59 eV for PIDTT-T-DFBT and PIDTCPDT-DFBT, respectively. The extinction coefficients of the polymer films were measured to evaluate the effect of conjugation length and torsion angle on the absorptivity of the polymers. Figure 1b shows a clear difference of extinction coefficient between the two polymers. The PIDTCPDT-DFBT possesses relatively high extinction coefficient which can be attributed to its high degree of planarity and enhanced wavefunction overlap between HOMO and LUMO level.

The electrochemical properties of both polymers were investigated using cyclic voltammetry and the results are shown in **Figure 2**. The highest occupied molecular orbital/lowest unoccupied molecular orbital (HOMO/LUMO) values of PIDTT-T-DFBT and PIDTCPDT-DFBT are calculated based on the onset of the redox potentials using the known energy level for ferrocene, which is 4.8 eV below the vacuum level.[24,25] The calculated HOMO and LUMO values for PIDTT-T-DFBT and PIDTCPDT-DFBT are (–5.15 and –3.20 eV) and (–5.05 and –3.28 eV), respectively.

To help understand the geometric and electronic properties of these polymers, density functional theory (DFT) calculations were performed at the B3LYP/6–31G (d) level by modeling the dimer of the polymers' repeating units. The HOMO and LUMO

Table 1. Optical and Electrochemical Properties of Polymers PIDTT-T-DFBT and PIDTCPDT-DFBT.

	UV-Vis absorption							
	Solution		Film			Cyclic Voltammetry		
Polymer	λ_{max} [nm]	λ_{onset} [nm]	λ_{max} [nm]	λ_{onset} [nm]	Bandgap	HOMO [eV]	LUMO [eV]	Bandgap
PIDTT-T-DFBT	572.05	664.20	592.00	699.53	1.77	–5.15	–3.20	1.95
PIDTCPDT-DFBT	671.72	744.73	682.15	776.90	1.59	–5.05	–3.28	1.77

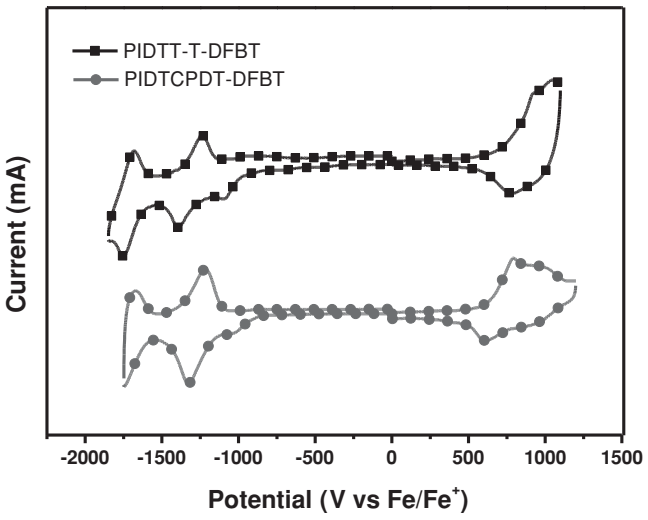

Figure 2. The cyclic voltammetry curves of polymers PIDTT-T-DFBT and PIDTCPDT-DFBT films.

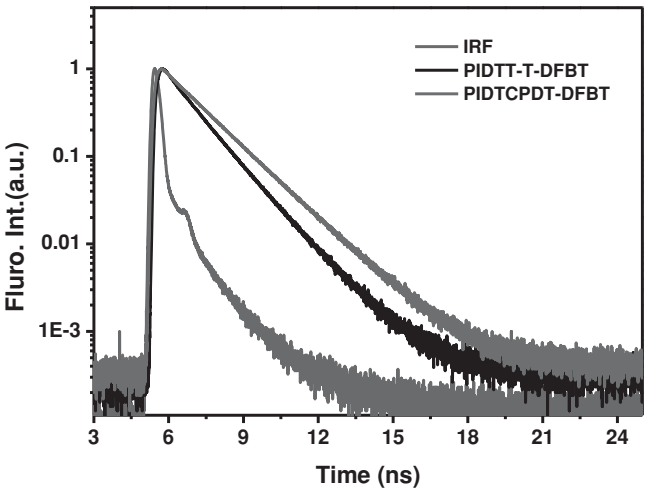

Figure 4. Time-resolved fluorescence of internal reference (IRF), PIDTT-T-DFBT and PIDTCPDT-DFBT in chlorobenzene solution. (The concentration for each polymer is about 0.1 mmol L^{-1}).

wave functions of the compounds are shown in **Figure 3**. The hexylphenyl side-chains are replaced with methyl-phenyl groups for simplicity of computation. For both oligomers, the HOMO wave functions are well delocalized along the polymer backbone, while their LUMO wave functions are localized on the acceptor unit. Meanwhile, the optimized geometries of both oligomers were also investigated. Figure 3 showed that PIDTT-T-DFBT has a fairly twisted backbone, indicating this polymer has higher rotational disorder. On the contrary, the covalently fastened two thiophene spacers to the IDTT donor resulted in a highly planar conformation with very small torsion angles of <0.7° (Figure S1, Supporting Information). This highly planar geometry would facilitate π-electron delocalization and enhance charge mobility.

Considering that vibrational and torsional motion of the polymers can drastically affect the radiative/non-radiative recombination processes in the excited state, time-resolved fluorescence spectra of PIDTT-T-DFBT and PIDTCPDT-DFBT in CB solutions were measured (**Figure 4**). The fluorescence lifetime, which refers to the average time of the molecule stays in its excited state before radioactively relaxed to the ground state, is an important parameter for fluorescence quantum yield.[26] The fluorescence decay of PIDTT-T-DFBT is much faster than that of PIDTCPDT-DFBT as shown in Figure 4. The fitted decay lifetime from the time-resolved PL data are 1.36 and 1.52 ns for PIDTT-T-DFBT and PIDTCPDT-DFBT, respectively. The twisted backbone of PIDTT-T-DFBT and its higher rotational freedom from less rigid thiophene bridges cause the shorter PL lifetime. The longer lifetime of the excited state in PIDTCPDT-DFBT should facilitate excitons to diffuse to the polymer-fullerene interface more efficiently for photocurrent generation.

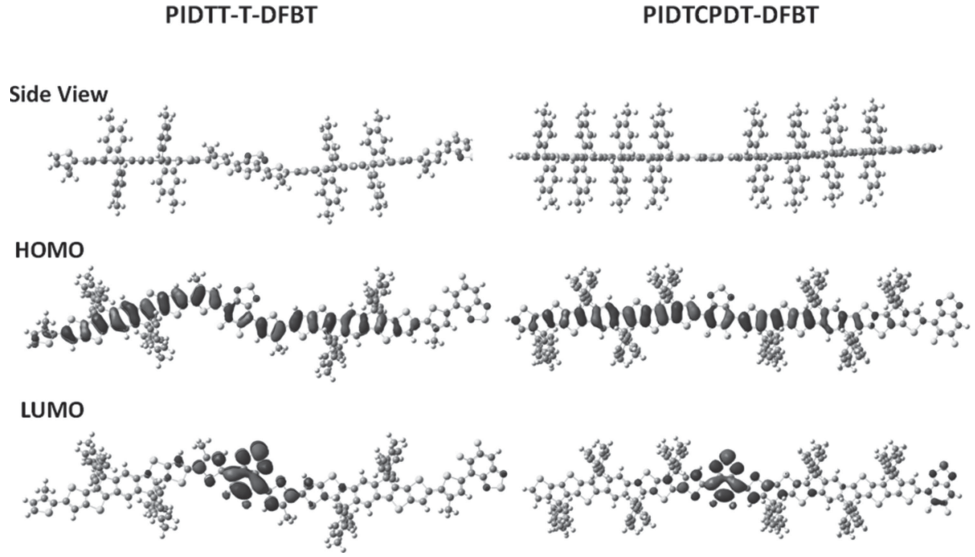

Figure 3. Molecular geometries and HOMO/LUMO wave functions of the dimer models of PIDTT-T-DFBT and PIDTCPDT-DFBT.

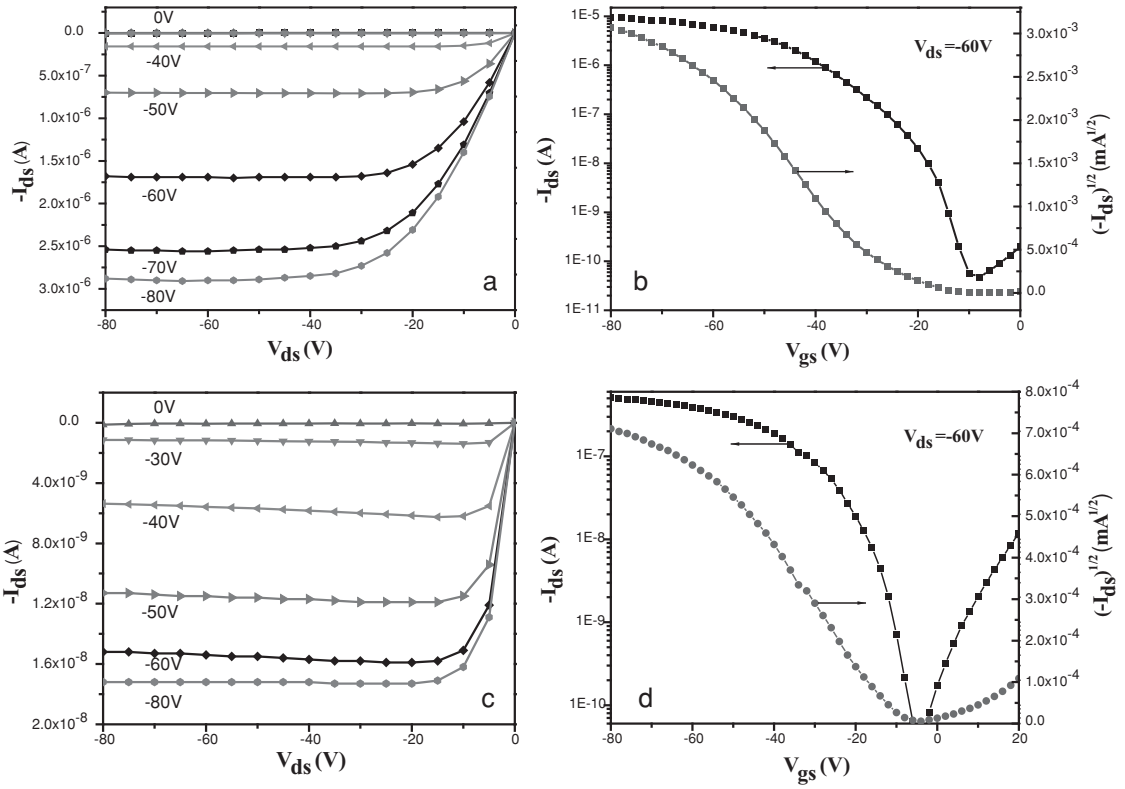

Figure 5. a,c) Output and b,d) transfer characteristics of a,b) PIDTCPDT-DFBT and c,d) PIDTT-T-DFBT.

The reorganizational energy due to geometric relaxation is also an important factor that affects charge transport in organic conjugated materials, since it influences the rate of charge hopping.[27–29] To examine this effect on these two polymers, additional DFT calculations were performed on the structurally optimized dimers. The hybrid B3LYP[30,31] functional and a 6–31G(d) basis set were used to obtain the optimized structures at the ground state. The vertical excitation energies were calculated at the optimized ground state geometries within the linear-response time-dependent DFT (LR-TDDFT) framework. The simulated absorption spectra were obtained by a Gaussian-function convolution (FWHM = 0.15 eV) of the vertical transition energies and oscillator strengths. The reorganizational energy was estimated using the adiabatic potential energy surfaces of the neutral and cationic species and can be expressed by Equation S1 and Figure S2 (Supporting Information). Due to increased orbital overlap and decreased torsion angles of PIDTCPDT-DFBT, a lower reorganizational energy was obtained for PIDTCPDT-DFBT (3.2 kcal mol^{-1}) compared to that calculated for PIDTT-T-DFBT (4.1 kcal mol^{-1}). This correlates well with decreased reorganizational energies observed when the planarity of polymer was enhanced[29] which should lead to higher hole-mobility in PIDTCPDT-DFBT.

Carrier mobility undoubted plays an important role in affecting the performance of a polymer solar cell since it is directly related to charge transport and recombination.[32] To examine if the reduced rotational disorder and reorganizational energy can indeed contribute to faster charge transport, PIDTT-T-DFBT and PIDTCPDT-DFBT based field-effect transistors (FETs) with a bottom-gate, top-contact device configuration were fabricated on an n-doped silicon wafer (**Figure 5** and **Table 2**). The calculated saturation hole mobility for PIDTT-T-DFBT and PIDTCPDT-DFBT is 1.6×10^{-3} and 2.4×10^{-2} cm^2 V^{-1} s^{-1}, respectively. The more than one order higher hole-mobility observed in PIDTCPDT-DFBT clearly shows the effectiveness of fusing the thiophene π-spacer onto PIDTT-T-DFBT. This enhancement supports the design hypothesis that longer effective conjugation length and improved planarity of the large fused ring systems will improve charge transport. This may also lead to higher fill factor in polymer solar cells.

The photovoltaic properties of both polymers were investigated in BHJ devices with a device configuration of ITO/PEDOT:PSS/polymer:$PC_{71}BM$/Bis-C_{60}/Ag under the illumination intensity of AM 1.5G at 100 mA cm^{-2}.[33,34] The J–V curves of the devices are shown in **Figure 6**a and the performance of these devices is summarized in **Table 3**. Due to reduced rotational disorder, longer exciton lifetime, enhanced charge mobility, and improved light absorption, PIDTCPDT-DFBT is expected to show better device performance than that of

Table 2. OFET Device Characteristics.

Polymer	$\mu_{sat,h}$ [cm^2 V^{-1} s^{-1}]	$I_{on/off,h}$	V_{th} [V]
PIDT-DFBT[a)]	2.3×10^{-3}	2.0×10^3	−32
PIDTT-T-DFBT	1.6×10^{-3}	1.6×10^4	−14
PIDTCPDT-DFBT	2.4×10^{-2}	2.0×10^5	−26

[a)]Data from our previous work.[22]

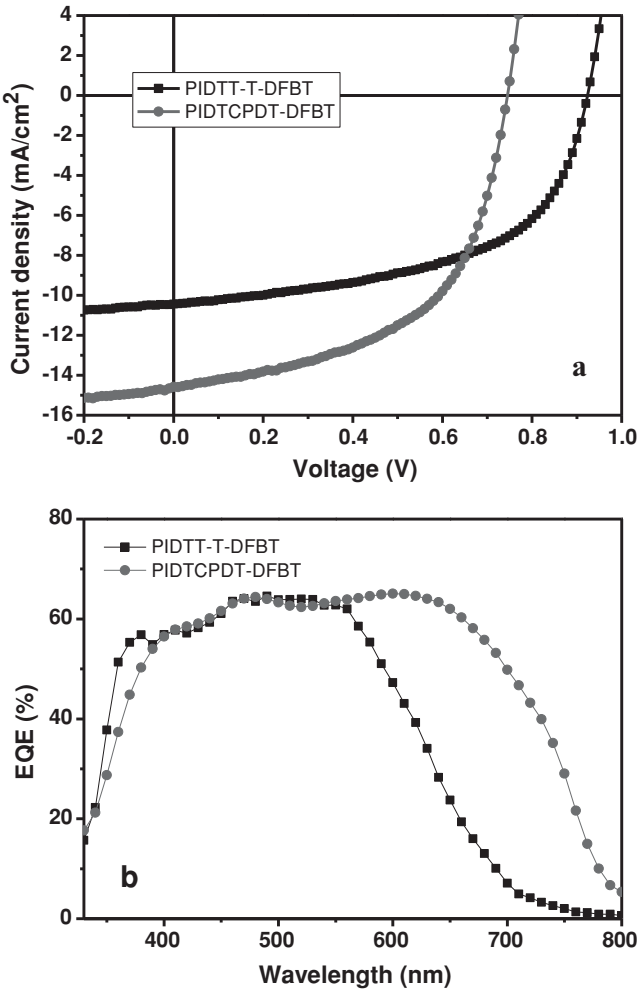

Figure 6. a) Current–voltage characteristics and b) EQE of photovoltaic devices based on PIDTT-T-DFBT and PIDTCPDT-DFBT with the blending ratio as 1:2.5 under illumination with 100 mW cm^{-2} (AM 1.5G).

PIDTT-T-DFBT. Indeed, the device based on PIDTCPDT-DFBT showed a respectable PCE of 6.46% with a V_{oc} of 0.75 V, a J_{sc} of 14.59 mA cm^{-2}, and a FF of 0.59. These results are higher than those obtained from using PIDTT-T-DFBT, has a lower PCE of 5.26% with a V_{oc} of 0.92 V, a significantly decreased J_{sc} of 10.40 mA cm^{-2}, and a FF of 0.55.

The increased J_{sc} and FF should be the result of better light-harvesting ability and higher charge mobility of PIDTCPDT-DFBT. However, a reasonably large difference in V_{oc} is observed due to the higher HOMO level of PIDTCPDT-DFBT. Since V_{oc} of a PSC is relevant to the difference between the HOMO level of polymer and the LUMO level of $PC_{71}BM$, the elevated HOMO level of the donor polymer results in lower V_{oc}.[35,36] To verify the origin of improved J_{sc}, the external quantum efficiencies (EQE) of these devices were measured and are shown in Figure 6b. The J_{sc} values calculated from the EQE curves under the standard AM 1.5G condition match well with those obtained from the *J–V* measurements. It should be noted that the blend of PIDTCPDT-DFBT and $PC_{71}BM$ showed significant photocurrent generated from the longer wavelengths absorption compared to that of PIDTT-T-DFBT-based devices, which agrees well with the absorption spectra of the polymer films. Additionally, quite smooth and featureless thin film morphology were observed in the atomic force microscopy (AFM) images of these polymer blends (Figure S3, Supporting Information), indicating good compatibility between these two polymers and $PC_{71}BM$.

Table 3. Photovoltaic properties of PSCs based on the polymers PIDTT-T-DFBT and PIDTCPDT-DFBT as the donor and $PC_{71}BM$ as the acceptor under the illumination of AM1.5G, 100 mW cm^{-2}.

Polymer	V_{oc} [V]	J_{sc} [mA cm^{-2}]	FF	PCE (%)[b)]
PIDT-DFBT[a)]	0.92 ± 0.01	10.87 ± 0.13	0.50 ± 0.01	5.10
PIDTT-T-DFBT	0.92 ± 0.01	10.40 ± 0.12	0.54 ± 0.02	5.26 (5.14)
PIDTCPDT-DFBT	0.75 ± 0.01	14.59 ± 0.16	0.59 ± 0.01	6.46 (6.32)

[a)]Data from our previous work;[8] [b)]Average PCE in the brackets.

3. Conclusions

In summary, two fused-ring, ladder-type conjugated polymers have been designed and synthesized. The fully fused PIDTCPDT-DFBT possesses lower band-gap, better planarity and lower reorganizational energy, and one-order higher hole-mobility. Solar cells made from PIDTCPDT-DFBT also showed higher power conversion efficiency of 6.46%. The short circuit current (J_{sc}) has also increased ≈40% from 10.40 mA cm^{-2} for a partially fused reference polymer, PIDTT-T-DFBT to 14.59 mA cm^{-2}. This is among the highest J_{sc} reported for the ladder-type polymers. These results show the strategy of extending conjugation length in fused-ring, ladder-type polymers is an effective way to reduce band-gap and improve charge transport for polymers to obtain higher photovoltaic efficiencies.

4. Experimental Section

Materials and Characterization: All chemicals, unless otherwise specified, were purchased from Aldrich and used as received. 2-bromothiophene-3-carboxylate, 2,5-dibromo-3,4-difluorobenzene, IDTT was synthesized according to the reported procedure.[22] Compound 2 were prepared according to the procedures described in the supporting information. UV-Vis spectra were measured using a Perkin-Elmer Lambda-9 spectrophotometer. The ^{1}H and ^{13}C NMR spectra were collected on a Bruker AV300 and 500 spectrometer operating at 300 and 125 MHz in deuterated chloroform solution with TMS as reference, respectively. Time of Flight MS- MALDI (TOF) MS were performed on a Bruker Autoflex II/Compass 1.0 from UW Department of Medicinal Chemistry. MS spectra were recorded on Bruker Esquire LC-Ion Trap. The molecular weight was measured by a Waters 1515 gel permeation chromatograph with a refractive index detector at room temperature (against polystyrene standards in THF). Thermal transitions were measured on a TA Instruments Q20–1066 Differential Scanning Calorimeter with a heating rate of 10 °C min^{-1}. Cyclic voltammetry of polymer film was conducted in acetonitrile with 0.1 M of tetrabutylammonium hexafluorophosphate using a scan rate of 100 mV s^{-1}. ITO, Ag/AgCl and Pt mesh were used as working electrode, reference electrode and counter electrode, respectively. AFM images under tapping mode were taken on a Veeco multimode AFM with a Nanoscope III controller. Time-resolved fluorescence spectra were carried on Fluorescence Lifetime Spectrometer (PicoQuant, FluoTime

100, PicoHarp 300). The laser excitation wavelengths are 405 nm. The laser pulse width is in the range of 70–90 ps.

Synthesis of compound 1: To a stirred solution of IDTT (408 mg, 0.4 mmol) in dry THF (10 mL) was added dropwise a 2.5 M solution of n-butyllithium in hexane (0.4 mL, 1.0 mmol) at −78 °C under argon atmosphere. After being stirred for 30 min at −78 °C, the resulting solution was warmed to room temperature and stirred for another 30 min. Then anhydrous zinc chloride (136 mg, 1.0 mmmol) in dry THF (10 mL) was added to the mixture dropwisely. The mixture was stirred at 0 °C for 1 h and then the cooling bath was removed. 2-bromothiophene-3-carboxylate (236 mg, 1.0 mmol) and $Pd(PPh_3)_4$ (46 mg, 0.04 mmol) were added directly. The reaction mixture was refluxed overnight. Upon completion, the reaction mixture was filtered over celite, extracted with ethyl acetate and then dried over anhydrous Na_2SO_4. The product was purified by silica gel chromatography to afford orange yellow solid (300 mg, 65%). ^{1}H NMR (300 MHz, d-$CDCl_3$, ppm): 7.79 (s, 2H), 7.51 (s, 2H), 7.49 (d, J = 6.0 Hz, 2H), 7.20–7.16 (m, 10H), 7.10–7.18 (m, 8H), 4.28 (q, J = 6.0 Hz, 4H), 2.56 (t, J = 7.5 Hz, 8H), 1.60–1.53 (m, 8H), 1.30–1.22 (m, 30H), 0.86 (t, J = 6.6 Hz, 12H). ^{13}C NMR (125 MHz, d-$CDCl_3$, ppm): 153.6, 146.2, 141.9, 141.7, 140.1, 136.1, 135.0, 134.7, 130.8, 128.5, 128.1, 127.9, 123.9, 122.4, 117.1, 66.0, 63.0, 60.8, 35.6, 31.7, 31.3, 29.2, 22.6, 14.2, 14.1.

Synthesis of IDTCPDT: To a solution of 4-hexyl-1-bromobenzene (376 mg, 1.6 mmmol) in THF (10 mL) at −78 °C was added n-BuLi (0.64 mL, 1.6 mmol, 2.5 M in hexane), the mixture was kept at −78 °C for 1 h. Then a solution of compound **1** (300 mg, 0.26 mmol) in THF (10 mL) was added slowly. After the addition, the mixture was stirred at room temperature overnight and then poured into water and extracted twice with ethyl acetate. The combined organic phase was dried over Na_2SO_4. After removing the solvent, the crude product was charged into three-neck flask. Acetic acid (20 mL) and concentrated H_2SO_4 (0.4 mL) were added and the mixture was refluxed for 2 h. Then the mixture was poured into water, extracted with ethyl acetate. The resulting crude compound was purified by silica gel column using a mixture of hexane/DCM as the eluent to give a red solid (192 mg, 40%). ^{1}H NMR (300 MHz, d-$CDCl_3$, ppm): 7.37 (s, 2H), 7.17–7.04 (m, 36H), 2.58 (t, J = 6.0 Hz, 16H), 1.60–1.53 (m, 16H), 1.28 (m, 48H), 0.87 (m, 24H). ^{13}C NMR (125 MHz, d-$CDCl_3$, ppm): 157.2, 153.1, 148.6, 146.7, 142.0, 141.8, 141.7, 140.4, 139.8, 137.7, 137.1, 136.2, 135.8, 134.5, 128.5, 128.1, 127.8, 126.3, 125.4, 123.3, 116.5, 63.0, 61.9, 35.6, 31.7, 31.3, 29.2, 22.6, 14.1. MS (MALDI) *m/z*: M^+, calcd for $C_{126}H_{142}S_6$, 1846.94; found, 1851.592.

Synthesis of IDTCPDTT-di-Tin: To a solution of IDTCPDT (185 mg, 0.10 mmol) in THF (10 mL) at −78 °C was added n-BuLi (0.10 mL, 0.25 mmol, 2.5 M in hexane). After the addition, the mixture was kept at −78 °C for 1 h and then warmed up to room temperature for another 30 min. After cooling back to −78 °C again, trimethyltin chloride (0.30 mL, 0.30 mmol, 1 M in hexane) was added dropwise. The resulting mixture was stirred overnight at room temperature. Then, it was poured into water and extracted with hexane. After drying over Na_2SO_4, the solvent was removed and ethanol was added. The precipitation was collected and dried as a solid (183 mg, 87%).^{1}H NMR (300 MHz, d-$CDCl_3$, ppm): 7.34 (s, 2H), 7.16–7.14 (m, 16H), 7.12–7.03 (m, 18H), 2.57 (q, J = 6.0 Hz, 16H), 1.60–1.53 (m, 16H), 1.28 (m, 48H), 0.87 (m, 24H), 0.35 (m, 18H). ^{13}C NMR (125 MHz, d-CDCl3, ppm): 159.1, 158.7, 153.0, 146.6, 141.7, 141.6, 141.5, 140.5, 140.2, 139.1, 139.0, 136.2, 135.0, 134.9, 128.4, 128.1, 127.9, 125.4, 123.3, 116.5, 63.0, 61.9, 35.6, 31.7, 31.3, 29.2, 22.6, 14.1, −7.9.

Polymerization of PIDTCPDT-DFBT: IDTCPDT-di-Tin (80 mg, 0.04 mmol) and DFBT-I_2 (16 mg, 0.04 mmol) were charged in a 50 mL three-neck flask under argon. After adding toluene (5 mL), the mixture was degassed by three freeze/pump/thew cycles to remove O_2. Then $Pd_2(dba)_3$ (1 mg) and P(o-tol)$_3$ (1 mg) were added. The mixture was degassed once more. Then the mixture was heated at 120 °C for 3 d. After cooling to RT, the mixture was poured into methanol. The precipitate was collected and washed by Soxhlet extraction sequentially with acetone, hexane, and chloroform. The remained solid in the filter was collected and dried (65 mg, 81%). ^{1}H NMR (500 MHz, $CDCl_3$, ppm): 8.31 (s, 2H), 7.39 (s, 2H), 7.24–7.17 (m, 16H), 7.16–7.08 (m, 16H), 2.56 (m, 16H), 1.28 (m, 48H), 0.87 (m, 24H). Molecular weight: M_n = 19.6 kDa, M_w = 42.1 kDa, PDI = 2.15.

Polymerization of PIDTT-T-DFBT. In a 25 mL two-necked flask was charged with IDTT-di-Tin (65 mg, 0.048 mmol) and the compound 2 (32 mg, 0.048 mmol) in a mixture of tolurene (10 mL). After being purged with argon for 30 min. $Pd_2(dba)_3$ (0.0024 mmol) and P(o-tol)$_3$ (0.0087 mmol) were added consequently. Then, the resulted mixture was heated in 110 °C for 48 h. After cooling to room temperature, the resulted mixture was precipitated by adding into methanol (50 mL) and filtered. The collected precipitate was subjected to Soxhlet extraction with methanol, hexanes, and chloroform. The high molecular weight part was collected and dried under vacuum. Purple solid was obtained (yield: 85%). ^{1}H NMR (500 MHz, d-$CDCl_3$, ppm): 8.13(s, 2H), 7.53(s, 2H), 7.46(s, 2H), 7.24 (m, 8H), 7.12(m, 8H), 2.86 (m, 4H), 2.57 (m, 8H), 1.73 (m, 4H), 1.72–1.60 (m, 8H), 1.51–1.43 (m, 12H), 1.34–1.28 (m, 24H), 1.03 (m, 6H), 0.86 (m, 12H). Molecular weight: M_n = 17.3 kDa, M_w = 32.9 kDa, PDI = 1.90.

Organic Field-Effect Transistor Fabrication: Polymer field-effect transistors based on PIDTCPDT-DFBT and PIDTT-T-DFBT were fabricated using the top-contact and bottom-gate geometry. A thermally grown 300 nm thickness of SiO_2 was purchased from Montco Silicon Technologies INC and used as the gate dielectric. The source/drain regions were defined by a 50 nm thickness of Au through a shadow mask, and the channel length (L) and width (W) is 20–50 and 1000 μm, respectively. Before gilding the devices, the oxide layer was passivated with a thin divinyltetramethyldisiloxanebis(benzocyclobutene) (BCB) buffer layer. BCB precursor solution in toluene was spun onto the silicon oxide and subsequently annealed at 250 °C overnight. The total capacitance density measured from parallel-plate capacitors was 10.6 nF cm^{-2}. Polymer solution (0.5 wt%) in o-DCB was first filtered through 0.2 μm syringe filters, spin-coated at a speed rate of 1000 rpm for 60 s onto the BCB-modified substrate, and then annealed at 130 °C for 10 min under nitrogen. Output and transfer characteristics of the transistor devices were performed in a N_2-filled glovebox using an Agilent 4155B semiconductor parameter S6 analyzer. The field-effect mobility was calculated in the saturation regime from the linear fit of $(I_{ds})^{1/2}$ vs V_{gs}. The threshold voltage (V_t) was estimated as the intercept of the linear section of the plot of $(I_{ds})^{1/2}$ vs V_{gs}.

Photovoltaic Device Fabrication: ITO-coated glass substrates (15 Ω sq^{-1}) were cleaned with detergent, de-ionized water, acetone, and isopropyl alcohol. A thin layer (≈ 35 nm) of PEDOT:PSS (Baytron P VP AI 4083, filtered at 0.45 μm) was first spin-coated on the pre-cleaned ITO-coated glass substrates at 5000 rpm and baked at 140 °C for 10 min under ambient conditions. The substrates were then transferred into an argon-filled glovebox. Subsequently, the polymer: $PC_{71}BM$ active layer (≈ 90 nm) was spin-coated on the PEDOT:PSS layer at 600 rpm from a homogeneously blended solution. The solution was prepared by dissolving the polymer and fullerene at weight ratios of 1:2.5 in o-dichlorobenzene with 3 wt% chloronaphthalene to a total concentration of 20 mg mL^{-1} at 80 °C overnight and then filtered through a PTFE filter (0.45 μm) before used. All of the substrates were placed on the hotplate at 110 °C for 10 min. After annealing, the substrates were briefly transferred out of the glovebox (total ambient exposure <10 min) and a 10 nm thick film of C_{60}-bis surfactant[33,34] (1 mg mL^{-1} in methanol) was spin-coated at 5 k rpm. The substrates were then transferred back into the glovebox and annealed at 110 °C for 5 min to remove any residual solvent prior to metal deposition. At the final stage, the substrates were pumped under high vacuum (< 2×10^{-6} Torr), and silver (100 nm) was thermally evaporated onto the active layer. Shadow masks were used to define the active area (10.08×10^{-2} cm^2) of the devices. The reported results are obtained from the average value of 20 devices.

Device Characterization: The un-encapsulated solar cells were tested under ambient conditions using a Keithley 2400 SMU and an Oriel Xenon lamp (450 W) with an AM1.5 filter. The light intensity was calibrated to 100 mW cm^{-2} using a calibrated silicon solar cell with a KG5 filter, which has been previously standardized as the National Renewable Energy Laboratory. The current-voltage (*I–V*) characteristics

of unencapsulated photovoltaic devices were measured under ambient conditions using a Keithley 2400 source-measurement unit. An Oriel xenon lamp (450 Watt) with an AM1.5 G filter was used as the solar simulator. The light intensity was set to 1 sun (100 mW cm^{-2}) using a calibrated Hamamatsu silicon diode with a KG5 color filter, which can be traced to the National Renewable Energy Laboratory (NREL). The EQE system uses a lock-in amplifier (Stanford Research Systems SR830) to record short-circuit current under chopped monochromatic light.

Supporting Information

Supporting Information is available from the Wiley Online Library or from the author.

Acknowledgements

The authors thank the support from the Air Force Office of Scientific Research (FA9550–09–1–0426), the Asian Office of Aerospace R&D (FA2386–11–1–4072), the Office of Naval Research (N00014–11–1–0300). A.K.-Y.J. thanks the Boeing Foundation for support. Y.L. thanks the State-Sponsored Scholarship for Graduate Students from China Scholarship Council.

Received: November 24, 2013
Revised: December 29, 2013
Published online: March 6, 2014

[1] Z. He, C. Zhong, S. Su, M. Xu, H. Wu, Y. Cao, *Nat. Photonics* **2012**, *6*, 591.
[2] H. Zhou, L. Yang, W. You, *Macromolecules* **2012**, *45*, 607.
[3] C.-P. Chen, S.-H. Chan, T.-C. Chao, C. Ting, B.-T. Ko, *J. Am. Chem. Soc.* **2008**, *130*, 12828.
[4] I. McCulloch, R. S. Ashraf, L. Biniek, H. Bronstein, C. Combe, J. E. Donaghey, D. I. James, C. B. Nielsen, B. C. Schroeder, W. Zhang, *Acc. Chem. Res.* **2012**, *45*, 714.
[5] H. Bronstein, D. S. Leem, R. Hamilton, P. Woebkenberg, S. King, W. Zhang, R. S. Ashraf, M. Heeney, T. D. Anthopoulos, J. d. Mello, I. McCulloch, *Macromolecules* **2011**, *44*, 6649.
[6] Y. Zhang, J. Zou, H.-L. Yip, K.-S. Chen, D. F. Zeigler, Y. Sun, A. K. Y. Jen, *Chem. Mater.* **2011**, *23*, 2289.
[7] J. Zhang, W. Cai, F. Huang, E. Wang, C. Zhong, S. Liu, M. Wang, C. Duan, T. Yang, Y. Cao, *Macromolecules* **2011**, *44*, 894.
[8] Y. Zhang, S.-C. Chien, K.-S. Chen, H.-L. Yip, Y. Sun, J. A. Davies, F.-C. Chen, A. K. Y. Jen, *Chem. Commun.* **2011**, *47*, 11026.
[9] J.-S. Wu, Y.-J. Cheng, M. Dubosc, C.-H. Hsieh, C.-Y. Chang, C.-S. Hsu, *Chem. Commun.* **2010**, *46*, 3259.
[10] Y.-J. Cheng, C.-H. Chen, Y.-S. Lin, C.-Y. Chang, C.-S. Hsu, *Chem. Mater.* **2011**, *23*, 5068.
[11] H.-H. Chang, C.-E. Tsai, Y.-Y. Lai, D.-Y. Chiou, S.-L. Hsu, C.-S. Hsu, Y.-J. Cheng, *Macromolecules* **2012**, *45*, 9282.
[12] J.-S. Wu, Y.-J. Cheng, T.-Y. Lin, C.-Y. Chang, P.-I. Shih, C.-S. Hsu, *Adv. Funct. Mater.* **2012**, *22*, 1711.
[13] H. Bronstein, R. S. Ashraf, Y. Kim, A. J. P. White, T. Anthopoulos, K. Song, D. James, W. Zhang, I. McCulloch, *Macromol. Rapid Commun.* **2011**, *32*, 1664.
[14] Z. Fei, R. S. Ashraf, Z. Huang, J. Smith, R. J. Kline, P. D'Angelo, T. D. Anthopoulos, J. R. Durrant, I. McCulloch, M. Heeney, *Chem. Commun.* **2012**, *48*, 2955.
[15] J.-S. Wu, Y.-Y. Lai, Y.-J. Cheng, C.-Y. Chang, C.-L. Wang, C.-S. Hsu, *Adv. Energy Mater.* **2013**, *3*, 457.
[16] Y.-J. Cheng, C.-H. Chen, T.-Y. Lin, C.-S. Hsu, *Chem. Asian J.* **2012**, *7*, 818.
[17] Y.-L. Chen, C.-Y. Chang, Y.-J. Cheng, C.-S. Hsu, *Chem. Mater.* **2012**, *24*, 3964.
[18] Y. Zhang, J. Zou, C.-C. Cheuh, H.-L. Yip, A. K. Y. Jen, *Macromolecules* **2012**, *45*, 5427.
[19] S. Albrecht, S. Janietz, W. Schindler, J. Frisch, J. Kurpiers, J. Kniepert, S. Inal, P. Pingel, K. Fostiropoulos, N. Koch, D. Neher, *J. Am. Chem. Soc.* **2012**, *134*, 14932.
[20] J. Hou, T. L. Chen, S. Zhang, H.-Y. Chen, Y. Yang, *J. Phys. Chem. C* **2009**, *113*, 1601.
[21] L. Dou, C.-C. Chen, K. Yoshimura, K. Ohya, W.-H. Chang, J. Gao, Y. Liu, E. Richard, Y. Yang, *Macromolecules* **2013**, *46*, 3384.
[22] Y.-X. Xu, C.-C. Chueh, H.-L. Yip, F.-Z. Ding, Y.-X. Li, C.-Z. Li, X. Li, W.-C. Chen, A. K. Y. Jen, *Adv. Mater.* **2012**, *24*, 6356.
[23] Y.-X. Xu, C.-C. Chueh, H.-L. Yip, C.-Y. Chang, P.-W. Liang, J. J. Intemann, W.-C. Chen, A. K. Y. Jen, *Poly. Chem.* **2013**, *4*, 5220.
[24] Y. Li, Z. Pan, Y. Fu, Y. Chen, Z. Xie, B. Zhang, *J. Polym. Sci., Part A: Polym. Chem.* **2012**, *50*, 1663.
[25] Y. Li, Z. Pan, L. Miao, Y. Xing, C. Li, Y. Chen, *Poly. Chem.* **2014**, *5*, 330.
[26] Y. Ren, J. W. Y. Lam, Y. Dong, B. Z. Tang, K. S. Wong, *J. Phys. Chem. C* **2005**, *109*, 1135.
[27] S. S. Zade, M. Bendikov, *Chem. Eur. J.* **2008**, *14*, 6734.
[28] X.-K. Chen, J.-F. Guo, L.-Y. Zou, A.-M. Ren, J.-X. Fan, *J. Phys. Chem. C* **2011**, *115*, 21416.
[29] G. R. Hutchison, M. A. Ratner, T. J. Marks, *J. Am. Chem. Soc.* **2005**, *127*, 2339.
[30] A. D. Becke, *J. Chem. Phys.* **1993**, *98*, 5648.
[31] P. J. Stephens, F. J. Devlin, C. F. Chabalowski, M. J. Frisch, *J. Phys. Chem.* **1994**, *98*, 11623.
[32] Y. Sun, S.-C. Chien, H.-L. Yip, Y. Zhang, K.-S. Chen, D. F. Zeigler, F.-C. Chen, B. Lin, A. K. Y. Jen, *J. Mater. Chem.* **2011**, *21*, 13247.
[33] K. M. O'Malley, C.-Z. Li, H.-L. Yip, A. K. Y. Jen, *Adv. Energy Mater.* **2012**, *2*, 82.
[34] C.-Z. Li, C.-C. Chueh, H.-L. Yip, K. M. O'Malley, W.-C. Chen, A. K. Y. Jen, *J. Mater. Chem.* **2012**, *22*, 8574.
[35] Y. Li, J. Zou, H.-L. Yip, C.-Z. Li, Y. Zhang, C.-C. Chueh, J. Intemann, Y. Xu, P.-W. Liang, Y. Chen, A. K. Y. Jen, *Macromolecules* **2013**, *46*, 5497.
[36] Y. Li, C.-Y. Chang, Y. Chen, Y. Song, C.-Z. Li, H.-L. Yip, A. K. Y. Jen, C. Li, *J. Mater. Chem. C.* **2013**, *1*, 7526.